Sustainable Energy & Fuels

ROYAL SOCIETY OF CHEMISTRY

PAPER

View Article Online
View Journal | View Issue

Cite this: *Sustainable Energy Fuels*, 2026, **10**, 1947

Thermophysical characterization of a new potential bio-oxygenate fuel formed by hexane, ethanol and diethyl carbonate

Ariel. Hernández,[ab] Marcela. Cartes[c] and Andrés. Mejía *[c]

The thermophysical characterization of a new potential bio-oxygenate fuel formed by ethanol, diethyl carbonate, and hexane is carried out by the direct determinations and theoretical predictions of the selected fundamental thermophysical properties (*i.e.*, vapor–liquid equilibria, dynamic viscosity, and surface tension) over the entire mole fraction range. Specifically, vapor–liquid equilibria (VLE) are reported at 94.00 kPa, over 330.0 K to 356.0 K, while liquid dynamic viscosity and surface tension are explored at 298.15 K and 101.3 kPa. The experimental VLE are modeled using the Perturbed Chain Statistical Associating Fluid Theory Equation of State (PC-SAFT EoS), which accounts for hydrogen bonding interactions between alcohol molecules and cross-interactions with the negative sites on the diethyl carbonate molecule. For the other two reported properties, the PC-SAFT EoS is coupled with free-volume theory and linear gradient theory, respectively. The advantage of this combined approach is that all required parameters are obtained from the corresponding pure fluids and binary mixtures that form the ternary mixture; therefore, the thermophysical properties of the ternary mixture are completely predicted. Based on experimental determinations and theoretical modeling, the VLE of the ternary mixture exhibits a positive deviation from Raoult's law, indicating zeotropic behavior under the conditions explored. The dynamic viscosities and surface tension display a monotonic behavior with the mole fraction. Finally, the combination of experimental measurements and molecular-based theoretical model provides a reliable framework to predict with physical sound and good accuracy these thermophysical properties over a broad range of temperature, pressure, and mole fractions that can be safely used to carry out further evaluations related to the use of this oxygenate fuel in complementary engine tests.

Received 31st January 2026
Accepted 19th March 2026

DOI: 10.1039/d6se00129g

rsc.li/sustainable-energy

1 Introduction

Considering the slowdown in the implementation of electromobility, the postponement of the normative that limits the fabrication and use of combustion engines, including gasoline and diesel engines, and the notorious increments of transportation, which is forecasted to grow at a rate of 1.8% every year by 2035,[1,2] it is necessary to explore new alternatives for renewable fuels and renewable additives for petroleum based fuels which can be directly used in the actual engines without significative modifications to support a cleaner gasoline and diesel combustion. Nowadays, there are synthetic and biomass-based routes to obtain renewable fuels,[3–7] where the synthetic routes, such as cyclopentyl methyl ether,[8] or those based on biomass sources where 2,5-dimethylfuran,[9] bioalcohols with low molecular weight alcohols (*i.e.*, methanol, ethanol, butanol, propanol), bioethers (*i.e.*, dimethyl ether, diethyl ether, methyl tertiary-butyl ether, and tertiary-amyl methyl ether), and organic linear carbonates-based bioesters (*i.e.*, dimethyl carbonate or DMC and diethyl carbonate or DEC) are classified as the most important alternatives. The latter are in the forefront of alternative biodiesel, where the principal advantage is their high boiling points, which produce very low or negligible emissions of particulate matter, CO, CO_2, and SO_x, mitigating the GHG emissions. For excellent accounts of the advantages, production, and use of DMC and DEC as engine fuels, the reader is redirected to works from Ren *et al.*,[10] Kozak *et al.*,[11] Shukla and Srivastava,[12] Pan *et al.*,[13] and Yang *et al.*,[14] and references therein. Based on these works, a potential oxygenate blend formed by combining two of these renewable chemical families will yield a promising biooxigenate blend for use as a direct fuel or incorporated into fossil fuels to reduce environmental impacts and improve engine performance.

Based on the benefits of biooxigenate blends for fuels and considering the reported results,[10–12,14] a potential but less-explored renewable blends can be mixtures formed from a bioalcohol and a carbonate-based bioester. According to Demirbas[3] and Nanda *et al.*,[5] an initial analysis for testing the quality of fuel blends is the evaluation of selected thermophysical

[a]*Facultad de Ingeniería y Negocios, Universidad de Las Américas, Concepción, 4030000, Chile*

[b]*Centro de Modelación Ambiental y Dinámica de Sistemas (CEMADIS), Universidad de Las Américas, Santiago, Chile*

[c]*Departamento de Ingeniería Química, Universidad de Concepción, POB 160-C, Correo 3, Bío-Bío, Concepción, Chile. E-mail: amejia@udec.cl; Tel: +56 412203897*

properties such as phase equilibrium, density, viscosity, surface tension, and then some general parameters such as fire and flash points, cloud and pour points, cetane number, iodine number, ash content, acid value should be evaluated.

Focused on the main thermophysical properties and considering the available experimental data,[15] it is possible to conclude that the vapor–liquid equilibria, the liquid density, and liquid dynamic viscosity for binary mixtures formed by bioalcohol and carbonates-based bioesters have been broadly explored, but the surface tension is less explored, except for the cases of 1-butanol + DMC[16] and 1-butanol + DEC,[17] and no previous experimental works have been devoted for the cases where these biooxigenate blends are mixing with a fossil fuel.

In order to contribute to filling some of the detected missing experimental information and predictions, this work focuses on the initial exploration of a biooxigenate blend formed by ethanol as a bioalcohol and diethyl carbonate as a bioester as an oxygenate additive for fossil fuels, which is represented by hexane. Specifically, we focus on the experimental determination and molecular-based predictions of three key thermophysical properties: vapor–liquid equilibria (VLE) at 94 kPa, liquid dynamic viscosity, and surface tension at 101.3 kPa and 298.15 K for the ternary mixture and the surface tension at 101.3 kPa and 298.15 K of DEC binary mixtures for which no previous experimental determinations or modeling have been carried out. The experimental determinations are complemented with a predictive theoretical framework based on the perturbed chain statistical association fluid theory (PC-SAFT),[18,19] coupled with the Free Volume Theory[20,21] and with the linear version of the square gradient theory (LGT).[22,23]

2 Experimental section

2.1 Materials

Hexane and dry ethanol were acquired from Merck, while diethyl carbonate (DEC) was purchased from Sigma-Aldrich. These chemical reagents were used here without further purification. Table 1 summarizes their technical specification reported by the suppliers.

2.2 Experimental devices

The purity of pure fluids used here (*i.e.*, ethanol, diethyl carbonate, and hexane) and the mole fractions for the liquid and vapor phases for the mixtures are measured by using a Varian 3400 chromatograph (GC) with a thermal conductivity detector (TCD) which is connected to a packed separation column of 3 m long and 0.3 cm in diameter filled with silicone SE-30 (10%) as the stationary phase. The temperatures were set at 493.15 K for the injector and the detector, and 503.15 K for the column. For the case of pure fluids, the GC peak area directly reports its mass fraction, whereas for the mixture, the GC peak areas are converted to mole fractions using a calibration curve that ensures an accuracy better than 0.001. Complementarily, the quality of the pure fluids is evaluated by direct measurements of six properties: water content, refractive indexes, liquid mass densities, liquid dynamic viscosity, and surface tension, all measured at 298.15 K and 101.3 kPa. Additionally, their normal boiling points are also measured at 101.3 kPa. In this work, water content is measured using a Metrohm Karl Fischer coulometer (model 831), with a reported uncertainty of 0.003 in mass fraction. The refractive indexes are measured at the Na *D* line using a Bellingham and Stanley multiscale automatic refractometer (model RFM 81), with an accuracy of $\pm 10^{-5}$ and a temperature accuracy of ± 0.01 K. The liquid mass densities are determined with an Anton Paar oscillating *U*-tube density meter (model 5000 DMA), with a resolution of $\pm 5 \times 10^{-3}$ kg m^{-3}. The liquid dynamic viscosities of pure fluids and the ternary mixture are measured using an Anton Paar Stabinger viscometer (model SVM 3001), which uses the Couette principle and reports dynamic viscosities with a resolution of $\pm 3.46 \times 10^{-3}$ mPa s, and a temperature accuracy of ± 0.01 K. Surface tension determinations for pure fluids and mixtures are carried out using a Sensadyne maximum differential bubble pressure tensiometer (model PC500-LV) with a resolution of ± 0.05 mN m^{-1} and ± 0.1 K. Finally, the normal boiling points of the pure fluids and the vapor–liquid equilibria for the ternary mixtures are measured using in an all-glass Fischer Labor and Verfahrenstechnik VLE cell (model 601) which operates according to the Guillespie principle. In this device, the pressure and temperature are controlled to within ± 0.01 kPa and ± 0.01 K, respectively.

Specific technical specifications of the devices, including calibration procedures and detailed experimental procedures, have recently been described by some of us.[16,24,25] Finally, the associated standard and combined expanded uncertainties of the measurements are calculated using the NIST procedure[26,27] as described in our previous works.[24,25]

3 Theoretical section

3.1 Consistency analysis of vapor–liquid equilibria

The reliability of the experimental determinations of vapor–liquid equilibria (VLE) must be validated using thermodynamic consistency tests. For ternary mixtures, one accepted standard

Table 1 Technical details of the pure fluids

Chemical name	Supplier	CAS	Mass fraction purity reported by supplier	Purification method
Ethanol	Merck	64-17-5	0.999	No
DEC	Sigma-Aldrich	105-58-8	0.995	No
Hexane	Merck	110-54-3	0.990	No

test is the D test proposed by Wisniak and Tamir.[28] In this test, the local deviation (D) and its maximum deviation (D_{max}) are evaluated for two consecutive experimental points, a and b, and they are declared consistent when $D < D_{max}$. Mathematically, D and D_{max} are given by the following expressions:

$$D = \sum_{i=1}^{3} (x_{ia} - x_{ib})(\ln \gamma_{ia} - \ln \gamma_{ib}) \quad (1)$$

$$D_{max} = \sum_{i=1}^{3} (x_{ia} + x_{ib}) \left(\frac{1}{x_{ia}} + \frac{1}{y_{ia}} + \frac{1}{x_{ib}} + \frac{1}{y_{ib}} \right) \Delta x + \sum_{i=1}^{3} (x_{ia} + x_{ib}) \frac{\Delta P}{P} + 2 \sum_{i=1}^{3} |\ln \gamma_{ib} - \ln \gamma_{ia}| \Delta x + \sum_{i=1}^{3} (x_{ia} + x_{ib}) B_j \left[(T_a + C_j)^{-2} + (T_b + C_j)^{-2} \right] \Delta T. \quad (2)$$

where, x_{ia}, x_{ib} and y_{ia}, y_{ib} are the liquid and the vapor mole fractions for component i at the a and b points, respectively. Δx, ΔP, and ΔT represent the experimental uncertainties in the measurements of mole fraction, pressure, and temperature, respectively. Considering the VLE cell and GC device, these uncertainties are $\Delta x = \pm 0.001$, $\Delta P = \pm 0.1$ kPa, $\Delta T = \pm 0.1$ K. B_j, and C_j represent the Antoine vapor pressure expression for pure fluids, which is given by the expression:

$$\log \left(P_i^0 / \text{kPa} \right) = A_i - \frac{B_i}{(T/K) + C_i} \quad (3)$$

In eqn (1) and (2), γ_{ia}, and γ_{ib} are the activity coefficients for component i at the a and b points, respectively. In this work, these activity coefficients are calculated using the modified Raoult's law:[29]

$$\gamma_i = \frac{y_i P}{x_i P_i^0} \quad (4)$$

In eqn (4) x_i, and y_i symbolize the mole fractions of component i in the liquid and the vapor phase, respectively. P represents the total pressure, whereas and P_i^0 is the pure component vapor pressure of component i. In this expression, the virial correction has been omitted due to the lack of information on the second virial coefficient for the pure DEC and the corresponding second virial coefficients for the involved binary mixtures that conform the ternary mixture (*i.e.*, ethanol + DEC, and DEC + hexane).

3.2 Modeling the isobaric vapor–liquid phase equilibria

The isobaric vapor–liquid phase equilibria is calculated using the traditional phase equilibria conditions (*i.e.*, $T^V = T^L = T^0$; $P^V = P^L = P^0$; $\mu_i^V = \mu_i^L$ with $i = 1, 2, \ldots, n_c$) which can be rewritten using the bubble-point temperature calculations expressed in terms of the Helmholtz energy density, f, and its derivatives:[30]

$$\left(\frac{\partial f}{\partial \rho_i} \right)_T^V = \left(\frac{\partial f}{\partial \rho_i} \right)_T^L; \quad i = 1, 2, 3 \quad (5)$$

$$\left[\rho \left(\frac{\partial f}{\partial \rho} \right)_T - f \right]^V = \left[\rho \left(\frac{\partial f}{\partial \rho} \right)_T - f \right]^L \quad (6)$$

$$P^0 = \left[\rho \left(\frac{\partial f}{\partial \rho} \right)_T - f \right] \quad (7)$$

where the superscripts V and L denote the vapor and the liquid bulk phases, respectively, and 0 denotes the equilibrium condition. T is the temperature, P is the pressure, x_i, and y_i represent the mole fraction for the component i in the liquid and the vapor phases, respectively, and ρ is the molar density. Eqn (5) is equivalent to the chemical potential equality of component i; eqn (6) represents the equality of pressure, and eqn (7) is the restriction of the isobaric condition.

In this work, f is described by the Perturbed Chain Statistical Associating Fluid Theory Equation of State (PC-SAFT) molecular-based equation of state (EoS),[18,19] where f is built from the sum of different contributions, such as the ideal gas contribution, molar Helmholtz energy of dispersion, molar Helmholtz energy of hard-sphere chain, and the association contribution for molar Helmholtz energy. The reader is redirected to the original works for the corresponding expressions,[18,19] or alternatively, to some of our previous works.[16,31,32] As an illustration, Fig. 1 sketches the pure fluid and the binary parameters present in PC-SAFT EoS.

According to Fig. 1, a molecule i interacting with a molecule j, where the PC-SAFT parameters for the pure fluids (i and j) are the following: m is the number of monomers or segments of the molecule (i.e., four segments in molecule i, and three segments in molecule j), σ is the diameter of each monomer, which is independent of the temperature, ε is the London dispersion energy parameter. On the other hand, to better understand the association scheme in molecules, this work uses the following nomenclature: $N(a,b)$, where N is the total number of association sites, a is the number of negative sites, and b is the number of positive sites. Thus, in Fig. 1, it is observed that the

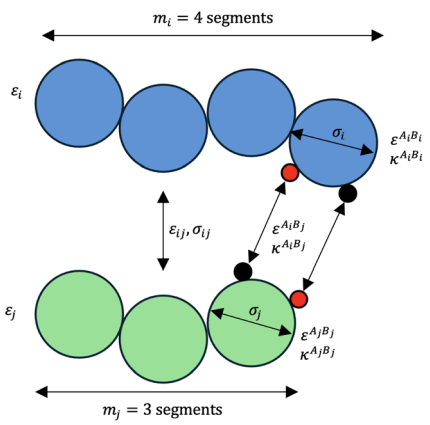

Fig. 1 Schematic representation of the interaction between molecule i, and molecule j, along with key PC-SAFT parameters. (blue circle) represents each segment of molecule i, (green circle) represents each segment of molecule j, (black circle) positive site in the molecule, (red circle) negative site in the molecule.

association scheme is 2(1, 1) in both molecules i, and j, and that hydrogen bonding interactions occur between the positive site of one molecule and the negative site of the other. Moreover, in each molecule, the parameters ε^{AB} and κ^{AB} represent the association energy and association volume parameters, respectively. For mixtures, the cross-parameters of diameter and dispersion energy are symbolized by σ_{ij} and ε_{ij} and are related to the pure components by the following combining rules:

$$\sigma_{ij} = (\sigma_i + \sigma_j)/2; \quad \varepsilon_{ij} = \sqrt{\varepsilon_i \varepsilon_j}(1 - k_{ij}) \tag{8}$$

where k_{ij} denotes the binary interaction parameter that corrects the geometric mean of the dispersion energy parameters of the pure fluids, obtained by fitting experimental phase-equilibrium data.

The effect of the association between molecules $i - j$ is considered from the binary parameters $\varepsilon^{A_iB_j}$ and $\kappa^{A_iB_j}$ which represent the cross-parameters of association energy and association volume, respectively. Mathematically, $\varepsilon^{A_iB_j}$ and $\kappa^{A_iB_j}$ are given by the expression:

$$\varepsilon^{A_jB_j} = \varepsilon^{A_iB_j}/2; \quad \kappa^{A_jB_j} = \kappa^{A_iB_j}\left(\sqrt{(\sigma_i\sigma_j)}\Big/\sigma_{ij}\right)^3 \tag{9}$$

3.3 Modeling the liquid dynamic viscosity

The liquid dynamic viscosity for the ternary mixture is predicted by using the Free Volume Theory (FVT) proposed by Allal *et al.*,[20,21] This theory establishes that liquid dynamic viscosity is composed of the sum of two contributions, namely dilute gas viscosity, η_i^0, whose expression was proposed by Chung *et al.*,[33] and residual viscosity, $\Delta\eta$, which is defined as:

$$\Delta\eta = \exp\left[B\left(\frac{\alpha + M_w P/\rho}{2RT}\right)^{1.5}\right]\left(\frac{\alpha + M_w P/\rho}{\sqrt{3M_w RT}}\right)\rho l \tag{10}$$

where P denotes pressure, M_w is the molecular weight, R is the universal gas constant, T is the temperature, B, α, and l are the adjustable model parameters and represent the free volume overlap, barrier energy, and the characteristic molecular length, respectively. In eqn (10), ρ is the density which is calculated here at T and P fixed using the PC-SAFT and eqn (7).

For mixtures, the FVT uses the following extension for η^0:

$$\eta^0 = \exp\left[\sum_{i=1}^{n_c} x_i \ln\left(\eta_i^0\right)\right] \tag{11}$$

Additionally, the adjustable parameters, B, α, and l are extended for mixtures using quadratic mixing rules:

$$\vartheta = \sum_{i=1}^{n_c}\sum_{j=1}^{n_c} x_i x_j \sqrt{\vartheta_i \vartheta_j}(1 - \psi_{ij}) \tag{12}$$

In eqn (12), ϑ symbolizes the parameter (*i.e.*, B, α, or l), and ψ_{ij} are adjustable binary parameters present in the residual viscosity of the mixture (*i.e.*, B_{ij}, α_{ij}, or l_{ij}). Form eqn (10)–(12), it is possible to observe that this model requires the experimental information on the liquid dynamic viscosity of the pure fluids and binary mixtures, but it is predictive for ternary mixtures.

3.4 Modeling of surface tension

The surface tension of the mixtures can be predicted using a linear version of the square gradient theory (LGT) proposed by Zuo and Stenby,[22,23] which assumes a linear profile of the components across the interfacial region. According to LGT, the surface tension, γ, in mixtures can be obtained from the following expression using the f given by the PC-SAFT EoS:

$$\gamma = \sqrt{2}\mathbb{C}\int_{\rho_{ref}^V}^{\rho_{ref}^L}\sqrt{f + \left[\rho\left(\frac{\partial f}{\partial \rho}\right)_T - f\right]^0 - \sum_{i=1}^{n_c}\rho_i\left(\frac{\partial f}{\partial \rho}\right)_T^0}\,d\rho_{ref} \tag{13}$$

where the pre-factor, $\mathbb{C}$, is given by the expression:

$$\mathbb{C} = \left(\sum_{i,j=1}^{n_c}\sqrt{c_i c_j}(1 - \beta_{ij})\frac{(\rho_i^L - \rho_i^V)}{\Delta\rho_{ref}}\frac{\left(\rho_j^L - \rho_j^V\right)}{\Delta\rho_{ref}}\right) \tag{14}$$

where c_i, and c_j are the influence parameters for pure fluids, which are obtained by applying eqn (13) for the case of pure fluids at fixed temperature, β_{ij} is a binary cross parameter obtained from the surface tension of the binary mixture formed by i and j. The superscript 0 denotes the equilibrium condition, ρ_{ref} is the reference density, and $\Delta\rho_{ref} = \max(\rho_i^L - \rho_i^V)$ with $i = 1, 2, \ldots, n_c$. From a computational point of view, the surface tension is calculated at a fixed temperature using the PC-SAFT EoS, and the equilibrium conditions are used to determine the integral limits corresponding to the bulk densities at phase equilibrium.

4 Results and discussion

In this section, the explored thermophysical properties (*i.e.*, phase equilibria, liquid dynamic viscosities, and surface tensions) for the pure fluids, binary mixtures, and the ternary mixture of the systems formed by ethanol, diethylcarbonate (DEC), and hexane are described. Specifically, the pure fluid properties are measured as quality indicators, and their values are also used to parameterize the theoretical models. For the binary mixtures, the experimental phase equilibria and liquid dynamic viscosities are taken from the available experimental data, as well as the surface tension for ethanol + hexane binary mixture, whereas the surface tensions for DEC-based binary mixtures are measured because no previous experimental data are available.[15,34] These determinations are then used to find the corresponding binary parameters. Finally, the phase equilibria, liquid dynamic viscosities, and surface tensions for the ternary mixture are measured and predicted using the proposed combined model.

4.1 Pure fluids

This section collects the measurements of selected thermophysical properties as quality chemical indicators for the pure fluids used in this work, as well as the thermophysical parameters required to validate and predict the phase equilibria, the liquid dynamic viscosities, and the surface tensions for the ternary ethanol + diethyl carbonate (DEC) + hexane mixture. Table 2 summarizes the measured values of the refractive indexes at the Na D line, liquid mass densities, liquid dynamic

Table 2 Experimental values of refractive indexes at Na *D* line (n_D), liquid mass densities ($\tilde{\rho}$), liquid dynamic viscosities (η), surface tensions (γ), and water content (wH_2O) at 298.15 K and 101.3 kPa, and the normal boiling points (T_b) at 101.3 kPa for ethanol, DEC, and hexane[a]

Fluid	n_D	$(\tilde{\rho})$ (kg m^{-3})	η (mPa s)	γ (mN m^{-1})	T_b (K)	$10^4 \times w\mathrm{H_2O}$ (mass fraction)
Ethanol	1.35940	785.16	1.1261	22.10	351.37	3.93
DEC	1.3836	969.23	0.721	25.20	399.13	0.20
Hexane	1.37374	655.19	0.2960	17.90	341.94	3.99

[a] The standard uncertainties, u, at the 0.68 level of confidence for temperature, pressure, and refractive index are $u(T) = 0.2$ K, $u(T_b) = 0.2$ K, $u(P) = 0.1$ kPa for T_b, $u(n_D) = 5.0 \times 10^{-4}$. Instrument declared standard uncertainties are $u(\rho) = 0.03$ kg m^{-3}, $u(\eta) = 2.0 \times 10^{-2}$ mPa s, $u(\sigma) = 0.3$ mN m^{-1}. The relative uncertainty for the water content is $u_r(w(\mathrm{H_2O})) = 0.003$. The combined expanded uncertainties using a 0.95 level of confidence ($k = 2$) are $U_c(T) = 0.4$ K, $U_c(T_b) = 0.4$ K, $U_c(P) = 0.2$ kPa, $U_c(n_D) = 10.0 \times 10^{-4}$, $U_c(\rho) = 0.06$ kg m^{-3}, $U_c(\eta) = 4.0 \times 10^{-2}$ mPa s, and $U_c(\sigma) = 0.6$ mN m^{-1}.

Table 3 Antoine constants (*A*, *B*, and *C*)

Fluid	*A*	*B*	*C*
Ethanol[35]	7.1533	1547.2702	−50.8767
DEC[17]	6.5665	1629.6470	−41.8125
Hexane[36]	6.2528	1310.6332	33.2066

Table 4 PC-SAFT pure fluid parameters[a]

Fluid	m	ε/k_B (K)	σ (Å)	ε^{AB}/k_B (K)	κ^{AB}	$N(a,b)$
Ethanol[a]	2.3827	198.24	3.1771	2653.4	0.032384	2(1,1)
DEC[c]	3.6622	255.64	3.5529	—	—	3(3,0)
Hexane[b]	3.0576	236.77	3.7983	—	—	0(0,0)

[a] The PC-SAFT parameters were taken from: (*a*) Gross and Sadowski;[19] (*b*) Gross and Sadowski;[18] (*c*) obtained in this work using the available experimental data for vapor pressure, P^0, and liquid mass density, $\tilde{\rho}$, in the NIST-TDE database,[37] using the objective function: $\min(m, \varepsilon, \sigma) = \sum_{i=1}^{n_p} [((P_i^{0,\mathrm{NIST}} - P_i^{0,\mathrm{SAFT}})/P_i^{0,\mathrm{NIST}})^2 + ((\tilde{\rho}_i^{\mathrm{NIST}} - \tilde{\rho}_i^{\mathrm{SAFT}})/\tilde{\rho}_i^{\mathrm{NIST}})^2]$.

viscosities, surface tensions, and water content at 298.15 K and 101.3 kPa, and the normal boiling points at 101.3 kPa.

Comparing the experimental determinations obtained in this work to those obtained in our previous works,[17,35,36] and the available reference data collected in the NIST-TDE database,[37] it is possible to state that all reported pure fluids properties display an absolute deviation not greater than 1%. Therefore, it is possible to state that the chemicals are adequate to carry out vapor–liquid equilibrium, liquid dynamic viscosity, and surface tension measurements.

Focused on validating experimental phase equilibrium determinations, the thermodynamic consistency test uses the Antoine coefficients (see Sec. 3.1). Their numerical values were obtained and validated in our previous works,[17,35,36] and summarized in Table 3.

As discussed in the theoretical section, vapor–liquid equilibria, liquid dynamic viscosities, and surface tensions are modeled using the PC-SAFT EoS, which uses pure fluid parameters, whose numerical values are summarized in Table 4 together with the selected associative schema.

Finally, the PC-SAFT EoS was coupled with the FVT and LGT to predict the liquid dynamic viscosities and the surface tensions, respectively. The FVT requires the free-volume overlap, B_i, barrier energy, α_i, and the characteristic molecular length parameters, l_i, while LGT needs the influence parameter, c_{ii}. The corresponding numerical values of the parameters involved in both theories are summarized in Table 5, which were calculated using the available experimental data in the NIST-TDE database.[37] Table 5 also includes the corresponding absolute average deviations (AAD) for the viscosity. The influence parameters were calculated using a single surface tension data point at 298.15 K.

From Tables 5 and it is possible to conclude that pure fluids can be correctly correlated using the PC-SAFT EoS coupled with FVT and LGT.

4.2 Binary mixtures

The binary mixtures that form the ternary mixture are ethanol + DEC, ethanol + hexane, and DEC + hexane. According to DECHEMA databases,[15] the vapor–liquid equilibria and the liquid dynamic viscosity of these binary mixtures have been previously measured. For surface tension, the available

Table 5 Free volume theory (FVT) and linear gradient theory parameters for pure fluids

	FVT				LGT
Fluid	α_i (J mol^{-1})	$10^3 \times B_i$	$10^3 \times l_i$ (Å)	% AAD, η[a]	$10^{19} \times c_{ii}$ (J m^5 m^{-2})
Ethanol	80 645.09	51.680	1.0617	0.05	0.53809
DEC	160 068.03	10.838	1.9727	0.10	4.23553
Hexane	196 743.26	4.3663	1.9297	0.12	3.68213

[a] % AAD, $\varphi = (100/n_p)\sum_{i=1}^{n_p} |\varphi_i^{exp} - \varphi_i^{cal}|/\varphi_i^{exp}$ with $\varphi = \eta$ or γ.

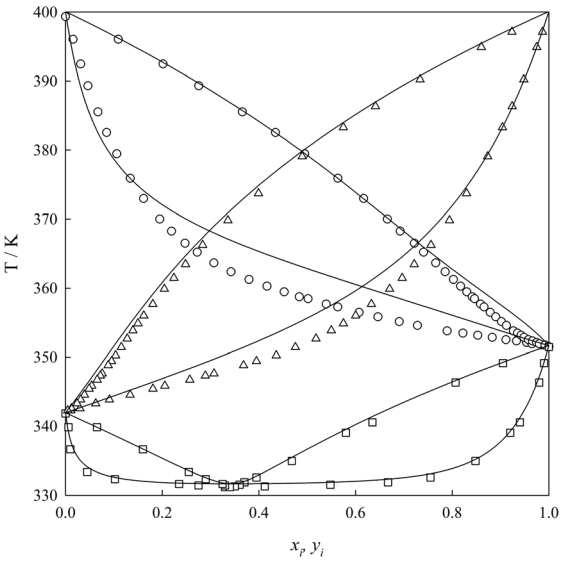

Fig. 2 Vapor–liquid equilibria at 101.3 kPa for ethanol (1) + DEC (2), ethanol (1) + hexane (3), and DEC (2) + hexane (3) mixtures. Experimental data: ethanol (1) + DEC (2): ○: Rodríguez *et al.*;[38] ethanol (1) + hexane (3): □: Sinor and Weber;[39] DEC (2) + hexane (3): △: Rodríguez *et al.*[40]. Continuous lines are the PC-SAFT modeling: ethanol (1) + DEC (2) with $k_{ij} = -0.0207$; ethanol (1) + hexane (3) $k_{ij} = 0.0338$; DEC (2) + hexane (3) $k_{ij} = 0.0200$.

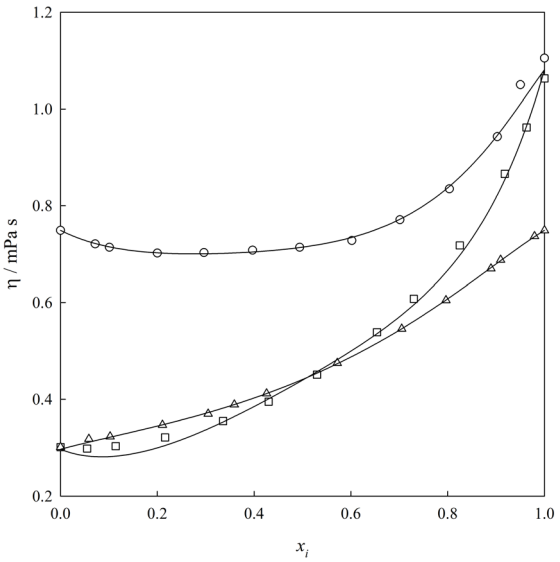

Fig. 3 Liquid dynamic viscosity for ethanol (1) + DEC (2), ethanol (1) + hexane (3) and DEC (2) + hexane (3) mixtures at 298.15 K and 101.3 kPa. Experimental data: ethanol (1) + DEC (2): ○: Rodríguez *et al.*;[41] ethanol (1) + hexane (3): □: Cartes *et al.*;[42] DEC (2) + hexane (3): △: Rodríguez *et al.*[43]. Continues lines are the PC-SAFT + FVT modeling: ethanol (1) + DEC (2) with $k_{ij} = -0.0207$ and $B_{ij} = 0.32650$, $\alpha_{ij} = 0.32284$, $l_{ij} = -1.28983$; ethanol (1) + hexane (3) $k_{ij} = 0.0338$, and $B_{ij} = 0.60653$, $\alpha_{ij} = 0.30154$, $l_{ij} = -0.64435$; DEC (2) + hexane (3) $k_{ij} = 0.0200$, and $B_{ij} = 0.53803$, $\alpha_{ij} = 0.093817$, $l_{ij} = -1.09263$.

experimental data are limited to the ethanol + hexane binary mixture. Therefore, in this section, experimental measurements of the surface tension for the ethanol + DEC and DEC + hexane binary mixtures are also included.

From a modeling point of view, the cross-binary parameters for PC-SAFT, FVT and LGT are obtained, and the results are compared with available experimental data.

4.2.1 Vapor–liquid equilibrium. Fig. 2 displays the experimental and modeling of the vapor–liquid equilibria (VLE) at 101.3 kPa for the three binary mixtures that form the ternary mixture, where it is possible to observe that the DEC-based binary mixtures display a zeotropy behavior with a positive deviation from the Raoult law. The ethanol + hexane binary mixture exhibits a minimum-temperature azeotrope with negative deviation from Raoult's law.

In order to model the VLEs, the interaction parameters (k_{ij}) have been obtained from the available experimental data using the following objective function:

$$\text{minOF} = \sum_{i=1}^{n_p} \left[\left(\left(T_i^{\text{exp}} - T_i^{\text{PC-SAFT}} \right) / T_i^{\text{exp}} \right)^2 + \left(y_{1,i}^{\text{exp}} - y_{1,i}^{\text{PC-SAFT}} \right)^2 \right] \quad (15)$$

Table 6 collects the numerical values of the interaction parameters and the corresponding statistical results of the fitting.

Based on the results exhibited in Fig. 2 and Table 6 and it is possible to conclude that PC-SAFT with $k_{ij} \neq 0$ is able to model the VLE of these three binary mixtures with an adequate agreement between experimental data and theoretical model, showing an overall deviation of AAD, $T = 0.46\%$ and $\Delta y_1 = 1.97\%$. However, it is noted that the calculated liquid compositions of DEC binary mixtures display an observable deviation from the experimental data, which is caused by the bubble T strategy. In this work, other VLE strategies (*e.g.*, bubble P and dew T, and dew P) were tested, but they exhibited similar global deviations.

Table 6 Optimal binary interactions parameters, k_{ij}, for the binary mixtures, and absolute average deviations in Temperature, % AAD T, and vapor mole fraction, % Δy_1

Binary mixture	k_{ij}	% AAD, T^a	% $\Delta y_1{}^b$
Ethanol (1) + DEC (2)	−0.0207	0.76	3.67
Ethanol (1) + hexane (3)	0.0338	0.14	0.98
DEC (2) + hexane (3)	0.0200	0.49	1.25

^{a} % AAD $T = (100/n_p) \sum_{i=1}^{n_p} \left| T_i^{\text{exp}} - T_i^{\text{SAFT}} \right| / T_i^{\text{exp}}$. ^{b} $\Delta y_1 = (100/n_p) \sum_{i=1}^{n_p} \left| y_{1,i}^{\text{exp}} - y_{1,i}^{\text{SAFT}} \right|$.

Table 7 Optimal binary parameters for FVT in the binary mixtures for the binary mixtures, and their absolute average deviations in viscosity, % AAD η

Binary mixture	B_{ij}	α_{ij}	l_{ij}	% AAD, η^a
Ethanol (1) + DEC (2)	0.32650	0.32284	−1.28983	0.70
Ethanol (1) + hexane (3)	0.60653	0.30154	−0.64435	2.18
DEC (2) + hexane (3)	0.53803	0.09382	−1.09263	0.42

[a] % AAD $\eta = (100/n_p)\sum_{i=1}^{n_p}\left|\eta_i^{exp} - \eta_i^{FVT}\right|/\eta_i^{exp}$.

4.2.2 Liquid dynamic viscosity. According to DECHEMA databases,[15] the liquid dynamic viscosity of these binary mixtures has been previously reported over the whole mole fraction range at a broad range of temperatures and pressures. Focused on the experimental conditions used in this work, Fig. 3 displays the corresponding experimental values together with the FVT calculations. The latter results were obtained using the density results from the PC-SAFT EoS and fitting the binary parameters involved in the FVT theory (see eqn (12)), whose numerical values are collected in Table 7.

From the results, it is possible to conclude that FVT coupled with PC-SAFT allows excellent modeling of the liquid dynamic viscosity (*i.e.*, % AAD, $\eta \leq 2$) From Fig. 3, it is possible to observe that the liquid dynamic viscosity increases as the molar fraction increases for the ethanol + hexane and DEC + hexane binary mixtures. For the ethanol + DEC mixture, the liquid dynamic viscosity initially decreases with the mole fraction and then increases, exhibiting a stationary point at $x \simeq 0.30$ for ethanol.

4.2.3 Surface tension. The surface tension of the binary mixtures has been less explored than the VLE and the liquid dynamic viscosity. According to the DECHEMA[15] and the Landolt-Bornstein[34] databases, the only available tensiometry data cover the surface tension of the ethanol + hexane binary mixture. In order to fill this gap and provide new experimental data on the surface tension for DEC-based binary mixtures, Table 8 reports the experimental data of surface tension as a function of the mole fraction for ethanol + DEC and DEC + hexane binary mixtures at 298.15 K and 101.30 kPa.

Table 8 Surface tensions for ethanol (1) + DEC (2) and DEC (2) + hexane (3) binary mixtures at 298.15 K and 101.30 kPa[a]

Ethanol (1) + DEC (2)		DEC (2) + hexane (3)	
x_1	γ (mN m^{-1})	x_2	γ (mN m^{-1})
0.00	27.89	0.000	17.91
0.05	27.88	0.046	17.98
0.09	27.73	0.084	18.26
0.19	27.30	0.189	18.90
0.30	26.84	0.294	19.59
0.40	26.39	0.395	20.04
0.50	26.01	0.499	20.87
0.60	25.39	0.598	21.75
0.69	24.61	0.699	22.76
0.80	23.84	0.805	24.22
0.90	22.79	0.901	25.90
0.96	22.39	0.957	27.03
1.00	22.10	1.000	27.89

[a] The instrument standard uncertainty, u, is $u(\sigma) = 0.3$ mN m^{-1}. The standard uncertainties, u, are $u(P) = 1.3$ kPa, $u(T) = 0.1$ K, and $u(x_1) = 0.005$. The combined uncertainties (using a level of confidence of 0.95 with $k = 2$) are $U_c(P) = 2.6$ kPa, $U_c(T) = 0.12$ K, $U_c(x_1) = 0.01$, and $U_c(\sigma) = 0.6$ mN m^{-1}.

Table 9 Optimal β_{ij} parameters for the binary mixtures obtained with PC-SAFT + LGT and their absolute average deviations in surface tension, % AAD γ

Binary mixture	% AAD, γ^a with $\beta_{ij} = 0$	β_{ij}	% AAD, γ^a
Ethanol (1) + DEC (2)	1.81	0.14369	0.40
Ethanol (1) + hexane (3)	3.04	0.21395	1.10
DEC (2) + hexane (3)	3.46	0.23938	0.72

[a] % AAD $\gamma = (100/n_p)\sum_{i=1}^{n_p}\left|\gamma_i^{exp} - \gamma_i^{LGT}\right|/\gamma_i^{exp}$.

In order to model the surface tensions of the binary mixtures with low deviations, it is necessary to fit the cross binary parameter involved in the LGT, β_{ij}, as it is described in eqn (13). The β_{ij} are obtained by the minimization of the following objective function:

$$OF = \sum_{i=1}^{n_p} \frac{\left(\gamma_i^{exp} - \gamma_i^{LGT}\right)^2}{\gamma_i^{exp}\cdot\gamma_i^{LGT}} \quad (16)$$

where the experimental values for ethanol + DEC and ethanol + DEC binary mixtures are reported in Table 8, while the experimental data on surface tension for ethanol + hexane were taken

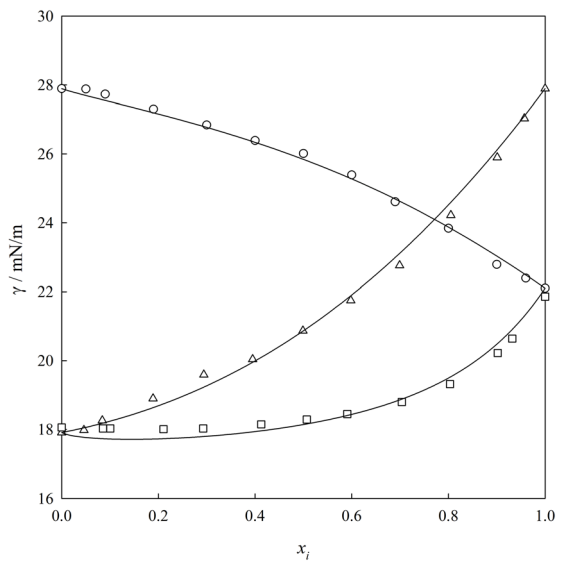

Fig. 4 Surface tension as a function of the mole fraction binary mixtures at 298.15 K and 101.3 kPa. Experimental data: ethanol (1) + DEC (2): ○: this work; ethanol (1) + hexane (3): □: Giner *et al.*;[44] DEC (2) + hexane (3): △: this work. Continues lines are the PC-SAFT + LGT modeling: ethanol (1) + DEC (2) with $k_{ij} = -0.0207$ and $\beta_{12} = 0.14369$; ethanol (1) + hexane (3) $k_{ij} = 0.0338$ and $\beta_{12} = 0.21395$; DEC (2) + hexane (3) $k_{ij} = 0.0200$, and $\beta_{12} = 0.23938$.

Table 10 Experimental determinations of the vapor–liquid equilibria (VLE) for ethanol (1) + DEC (2) + hexane (3) ternary mixture at 94.0 kPa[a]

T (K)	x_1	x_2	y_1	y_2
338.65	0.763	0.143	0.539	0.033
341.45	0.629	0.284	0.572	0.054
347.48	0.486	0.457	0.641	0.085
350.93	0.350	0.592	0.631	0.107
355.77	0.228	0.716	0.582	0.169
355.63	0.174	0.757	0.531	0.158
344.93	0.198	0.599	0.383	0.098
333.58	0.678	0.105	0.414	0.021
332.08	0.731	0.043	0.397	0.010
343.00	0.354	0.485	0.465	0.076
336.83	0.451	0.282	0.401	0.041
347.56	0.150	0.613	0.558	0.114
335.68	0.203	0.284	0.652	0.041
333.58	0.320	0.192	0.634	0.028
331.73	0.510	0.100	0.623	0.016
333.81	0.404	0.202	0.613	0.027
337.03	0.289	0.334	0.603	0.046
333.43	0.185	0.189	0.671	0.028
330.98	0.312	0.078	0.660	0.012
331.37	0.193	0.081	0.681	0.013
333.32	0.068	0.108	0.739	0.020
332.42	0.106	0.110	0.708	0.018

[a] T denotes temperature; x_1, and x_2 are mole fractions in the liquid phase for ethanol and DEC, respectively. y_1, and y_2 are mole fractions in the vapor phase for ethanol and DEC, respectively. Standard uncertainties, u, are $u(P) = 0.1$ kPa, $u(T) = 0.2$ K, and $u(x_i) = u(y_i) = 0.005$. The combined expanded uncertainties using a 0.95 level of confidence ($k = 2$) are $U_c(P) = 0.2$ kPa, $U_c(T) = 0.4$ K, and $U_c(x_i) = U_c(y_i) = 0.01$.

from Giner *et al.*,[44] Table 9 summarizes the obtained results with $\beta_{ij} = 0$ and $\beta_{ij} \neq 0$ and the corresponding absolute average deviations, % AAD γ.

As shown in Table 9, the PC-SAFT with LGT with $\beta_{ij} = 0$ demonstrates a good quantitative agreement between the theoretical and experimental data. The adjustment approach

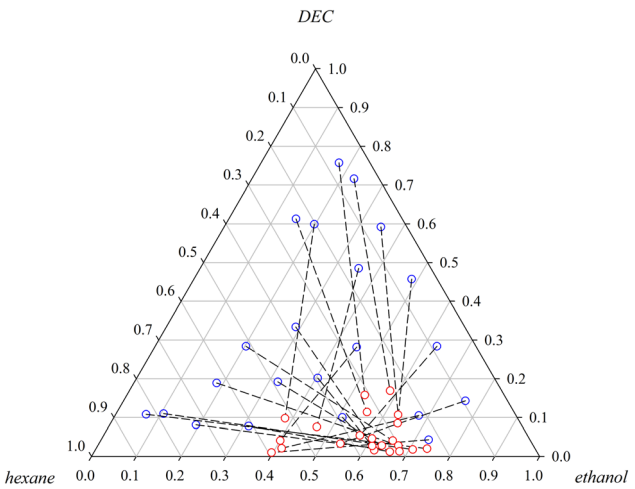

Fig. 5 Measured data of the vapor–liquid phase equilibria (VLE) for the ethanol (1) + DEC (2) + *n*-hexane (3) ternary mixture at 94.00 kPa. (◯) liquid phase; (◯) vapor phase; (- - -) tie line.

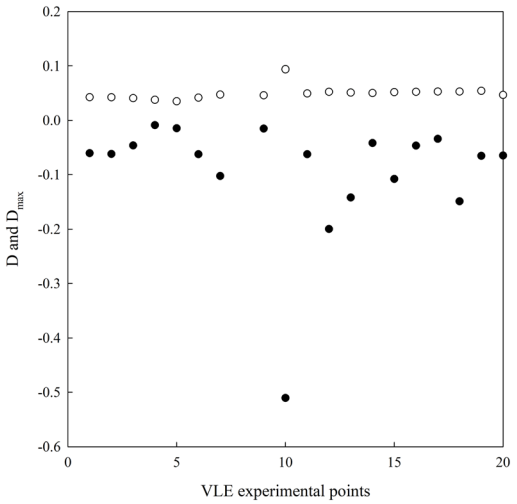

Fig. 6 Thermodynamic consistency D test. D and D_{max} *vs.* number of experimental points for the ethanol (1) + DEC (2) + hexane (3) ternary mixture at 94.0 kPa. ●: D; ○: D_{max}.

significantly reduces the overall deviation from 2.77% in the predictive approach to 0.74% in a correlative approach. This indicates that non-zero β_{ij} values effectively fit the experimental surface tension for all three binary mixtures.

Fig. 4 displays the experimental determinations and theoretical modeling of the surface tensions for the three binary mixtures.

From Fig. 4, it is observed that the variation of surface tension with the mole fraction is well correlated with the PC-SAFT + LGT.

4.3 Ternary mixture

Based on the DECHEMA databases,[15] the vapor–liquid equilibria (VLE), the liquid dynamic viscosity, and the surface tension have not been experimentally measured for this ternary mixture. In this section, these thermophysical properties are reported experimentally and theoretically predicted using the PC-SAFT EoS coupled with FVT for viscosity and LGT for surface tensions, which use only pure and binary parameters.

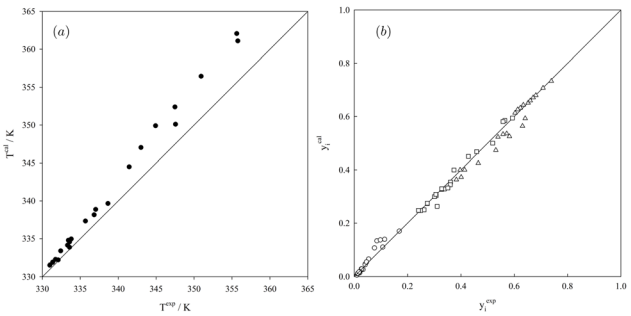

Fig. 7 Parity plots of the vapor–liquid equilibria for the ethanol (1) + DEC (2) + *n*-hexane (3) ternary mixture at 94.00 kPa. (a) Equilibrium temperature: ● (b) Vapor mole fractions: △: ethanol; ○: DEC; □: *n*-hexane.

Table 11 Statistical deviation in bubble point calculations for the ethanol (1) + DEC (2) + *n*-hexane (3) ternary mixture at 94.00 kPa

% AAD, T^a	% $\Delta y_1{}^b$	% $\Delta y_2{}^b$
0.66	2.92	3.55

^{a} % AAD $T = (100/n_P)\sum_{i=1}^{n_p}\left|T_i^{exp} - T_i^{SAFT}\right|/T_i^{exp}$. ^{b} % $\Delta y_i = (100/n_p)\sum_{j=1}^{n_p}\left|y_{i,j}^{exp} - y_{i,j}^{SAFT}\right|$.

Experimental measurements of the VLE have been carried out at 94 kPa whose numerical data are summarized in Table 10 and illustrated in Fig. 5 together with the corresponding tie lines.

From Fig. 5, it is possible to conclude that this ternary mixture behaves as a zeotropy mixture within the measurement range. Additionally, the computed activity coefficients from the modified Raoult law (see eqn (4)) show a positive deviation, $\gamma_i > 1$, implying $g^E = \sum_{i=1}^{3} \ln \gamma_i > 0$ in the whole mole fraction range. Additionally, it is possible to observe that as the mixture is diluted in DEC, the mixture tends to form an azeotrope, which is finally formed in the ethanol + hexane binary mixture.

To validate the reliability of the reported VLE data for this ternary system, the thermodynamic consistency of them is evaluated by using the *D* test (see eqn (1) and (2)) and the results are illustrated in Fig. 6 where it is possible to conclude that the VLE data fulfilled the thermodynamic consistency criteria (*i.e.*, $D < D_{max}$).

In order to evaluate the capability of the PC-SAFT EoS to predict the experimental VLE only using the pure parameters (see Table 4) and cross binary parameter (see Table 6), Fig. 7 *a* and *b* illustrate the corresponding parity plots for temperature (Fig. 7a) and vapor mole fractions (Fig. 7b) which are calculated from eqn (5)–(7).

From Fig. 7 *a* and *b*, it is possible to observe that the predictions can be considered acceptable when compared to experimental data. Complementarily, Table 11 presents the corresponding statistical deviations obtained from bubble-point calculations, which confirm the PC-SAFT EoS's capability to predict VLE.

Finally, Fig. 8 shows the PC-SAFT EoS predictions of the VLE in an isotherm map phase diagram (*i.e.*, $T - x_1 - x_2$) for the ternary system at 94.00 kPa. From this representation, it is possible to observe the azeotropy coordinates for the ethanol + hexane binary mixture (point A), and this diagram confirms that no ternary azeotrope is present in the ternary mixture.

Based on the VLE results from the PC-SAFT EoS, it is possible to state its high capability to predict VLE, providing a trustworthy model for exploring other isobaric conditions, such as those needed for industrial plant applications (*i.e.*, 70 kPa to 120 kPa).[6]

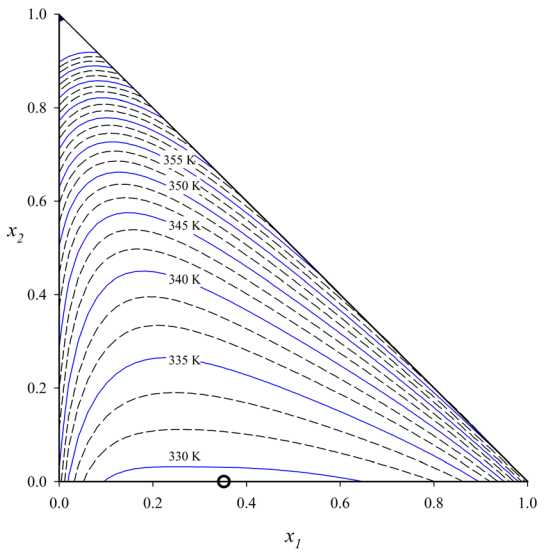

Fig. 8 Predicted bubble temperature diagram of the ethanol (1) + DEC (2) + *n*-hexane (3) ternary mixture at 94.00 kPa. The isolines are obtained from the PC-SAFT EoS with the binary parameters reported in Table 6. (○) Binary azeotrope for ethanol (1) + *n*-hexane (3) mixture ($x_1{}^{Az} = 0.345$, and $T^{Az} = 331.63$ K).

Table 12 Experimental determinations of the liquid dynamic viscosity for ethanol (1) + DEC (2) + hexane (3) ternary mixture at 298.15 K and 101.30 kPa[a]

x_1	x_2	η (mPa s)	x_1	x_2	η (mPa s)
0.115	0.787	0.602	0.093	0.507	0.420
0.192	0.712	0.593	0.187	0.408	0.387
0.308	0.592	0.582	0.304	0.294	0.389
0.403	0.505	0.588	0.392	0.196	0.400
0.507	0.396	0.594	0.503	0.096	0.439
0.592	0.307	0.608	0.098	0.396	0.362
0.703	0.196	0.641	0.195	0.404	0.390
0.810	0.099	0.725	0.309	0.292	0.399
0.115	0.689	0.524	0.387	0.195	0.403
0.199	0.609	0.514	0.503	0.095	0.435
0.305	0.508	0.510	0.095	0.401	0.363
0.405	0.398	0.503	0.204	0.297	0.353
0.493	0.308	0.513	0.292	0.197	0.359
0.609	0.196	0.544	0.397	0.092	0.389
0.701	0.100	0.593	0.109	0.227	0.330
0.093	0.611	0.460	0.205	0.197	0.338
0.198	0.503	0.441	0.292	0.096	0.355
0.298	0.396	0.432	0.099	0.195	0.319
0.396	0.298	0.449	0.199	0.091	0.334
0.499	0.192	0.455	0.096	0.095	0.315
0.591	0.098	0.497			

[a] η denotes liquid dynamic viscosity; x_1, and x_2 are mole fractions in the liquid phase for ethanol and DEC, respectively. The instrument standard uncertainty, *u*, is $u(\eta) = 2.0 \times 10^{-2}$ mPa s. The standard uncertainties, *u*, are $u(P) = 1.3$ kPa, $u(T) = 0.1$ K, and $u(x_1) = u(x_2) = 0.005$. The combined uncertainties (using a level of confidence of 0.95 with $k = 2$) are $U_c(P) = 2.6$ kPa, $U_c(T) = 0.2$ K, $U_c(x_1) = U_c(x_2) = 0.01$$, and $U_c(\eta) = 4.0 \times 10^{-2}$ mPa s.

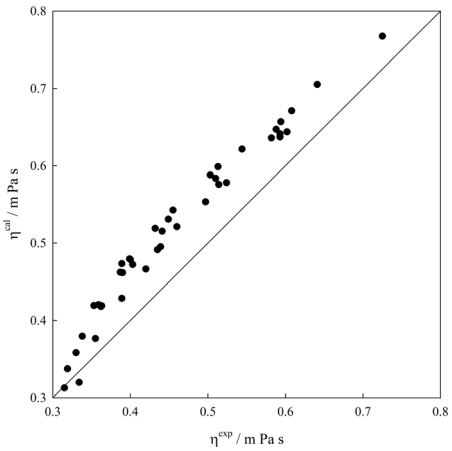

Fig. 9 Liquid dynamic viscosity parity plot for the ethanol (1) + DEC (2) + hexane (3) ternary mixture at 298.15 K and 101.325 kPa. ●: Free Volume Theory (FVT). The experimental data are presented in Table 12.

Complementary to the VLE, Table 12 collects the experimental measurements for the liquid dynamic viscosity for the ternary mixture at 298.15 K and 101.30 kPa, and Fig. 9 exhibits the corresponding parity plot, where it is possible to observe the performance of PC-SAFT coupled to FVT to predict its behavior.

From this Figure, it is possible to conclude that FVT over-predicts the experimental measurements with an absolute average deviation of 12.91%. This moderate-to-high deviation can be attributed to the high value of deviation observed for the ethanol + hexane binary mixture. Despite the moderately high global deviation, the model provides a route to obtain a complete description of the liquid dynamic viscosity for this ternary mixture, as illustrated in Fig. 10. The capability of the viscosity model for biofuels with respect to composition and temperature is relevant because it affects the operation of fuel injection equipment. In fact, at low temperatures, the viscosity increases, which affects fuel fluidity, whereas high viscosity leads to poorer fuel spray atomization and less accurate fuel injector operation.[3]

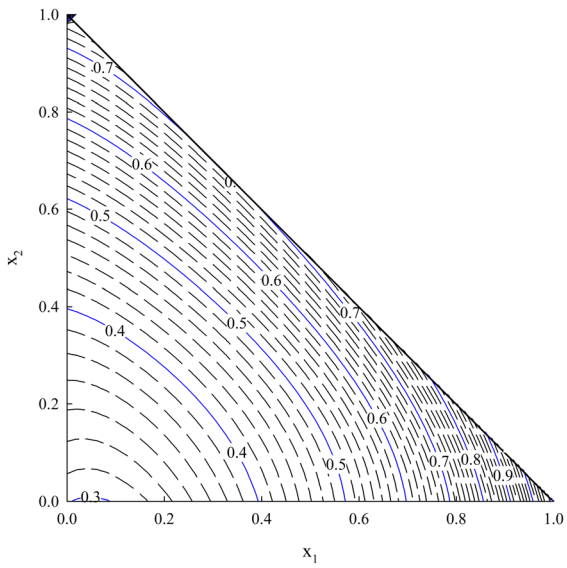

Fig. 10 Predicted liquid dynamic viscosity, η in mPa s, for the ethanol (1) + DEC (2) + hexane (3) ternary mixture at 298.15 K and 101.325 kPs. The isolines are obtained from the PC-SAFT EoS + FVT with the binary parameters reported in Tables 6 and 7

Table 13 Experimental determinations of the surface tension for ethanol (1) + DEC (2) + hexane (3) ternary mixture at 298.15 K and 101.30 kPa[a]

x_1	x_2	γ (mN m^{-1})	x_1	x_2	γ (mN m^{-1})
0.102	0.813	25.68	0.331	0.256	19.84
0.227	0.688	25.05	0.375	0.197	18.49
0.358	0.555	24.49	0.432	0.134	19.09
0.489	0.416	23.98	0.438	0.127	18.65
0.624	0.276	22.90	0.010	0.542	24.07
0.749	0.141	22.01	0.477	0.075	18.03
0.177	0.650	23.58	0.048	0.491	20.89
0.093	0.730	23.97	0.083	0.442	19.12
0.252	0.568	22.94	0.130	0.391	20.28
0.352	0.464	22.79	0.229	0.259	20.15
0.463	0.346	21.68	0.192	0.286	20.02
0.566	0.236	20.79	0.336	0.120	19.17
0.672	0.112	20.36	0.061	0.371	19.85
0.027	0.711	22.83	0.337	0.082	19.19
0.095	0.641	22.03	0.158	0.233	19.24
0.181	0.539	21.64	0.047	0.342	21.09
0.300	0.403	20.92	0.265	0.124	18.52
0.422	0.262	20.27	0.268	0.100	18.91
0.556	0.109	19.72	0.173	0.192	18.87
0.070	0.560	21.37	0.074	0.246	18.77
0.070	0.556	20.31	0.168	0.129	20.09
0.157	0.465	19.88	0.152	0.117	18.68
0.156	0.465	21.17	0.096	0.122	18.61
0.035	0.582	21.23	0.060	0.120	18.87
0.245	0.365	19.27	0.109	0.058	18.16
0.245	0.364	20.97	0.014	0.140	18.51
0.158	0.448	20.82	0.130	0.020	17.94
0.267	0.328	19.27	0.093	0.050	18.25
0.333	0.256	19.10			

[a] γ denotes surface tension; x_1, and x_2 are mole fractions in the liquid phase for ethanol and DEC, respectively. The instrument standard uncertainty, u, is $u(\sigma) = 0.3$ mN m^{-1}. The standard uncertainties, u, are $u(P) = 1.3$ kPa, $u(T) = 0.1$ K, and $u(x_1) = u(x_2) = 0.005$. The combined uncertainties (using a level of confidence of 0.95 with $k = 2$) are $U_c(P) = 2.6$ kPa, $U_c(T) = 0.12$ K, $U_c(x_1) = U_c(x_2) = 0.01$, and $U_c(\sigma) = 0.6$ mN m^{-1}.

Finally, the tensiometry measurements for the ternary mixture as a function of the liquid mole fractions at 298.15 and 101.3 kPa are summarized in Table 13.

Based on the theoretical approach, the surface tensions of the ternary mixture are fully predicted by using the LGT coupled with the PC-SAFT EoS. As described before, this approach uses only the pure parameters (see Table 5) and the binary parameters (see Table 9). In order to compare the performance of the theoretical approach for the ternary mixture, Fig. 11 shows the surface tension parity plot, where the LGT + PC-SAFT EoS reproduces the experimental values with a very low deviation of 2.69%.

Finally, Fig. 12 displays the predicted contour plot of the surface tension of the ternary mixture as a function of the liquid

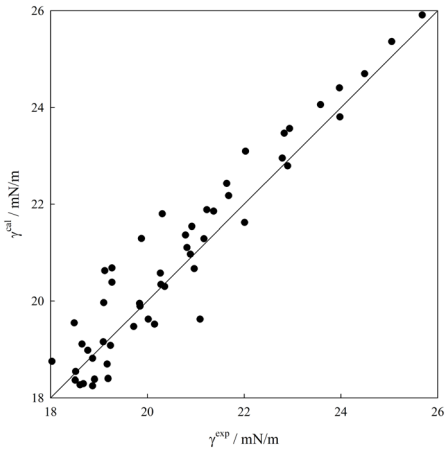

Fig. 11 Surface tension parity plot for the ethanol (1) + DEC (2) + hexane (3) ternary mixture at 298.15 K and 101.325 kPa. ●: Linear version of the square gradient theory (LGT). The experimental data are presented in Table 13.

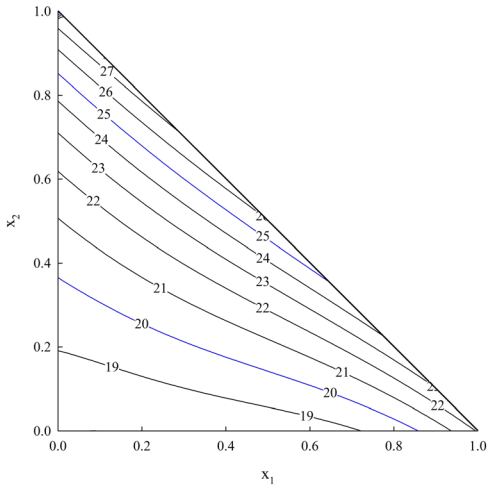

Fig. 12 Predicted surface tension, γ in mPa s, for the ethanol (1) + DEC (2) + hexane (3) ternary mixture at 298.15 K and 101.325 kPs. The isolines are obtained from the PC-SAFT EoS + FVT with the binary parameters reported in Tables 6 and 5

mole fractions at 298.15 K and 101.3 kPa, where it is possible to observe the variation of the surface tension in the whole liquid mole fraction range.

Similar to viscosity, the accurate prediction of the surface tension in biofuels plays a key role in the atomization process. In fact, the atomization quality increases with the reduction of surface tension.[45]

5 Conclusion

Based on current environmental regulations, high levels of unburned fuels, and dependence on fossil fuels, the exploration of alternative oxygenate mixtures for fuels has been motivated by the need for renewable, less-polluting oxygenate additives. In this work, a new potential bio-oxygenated mixture is explored from the thermophysical viewpoint, where the vapor–liquid phase equilibria, liquid dynamic viscosities, and surface tensions for the ethanol + DEC + *n*-hexane ternary mixture are experimentally measured and theoretically predicted. Specifically, the vapor–liquid phase equilibrium was explored at 94 kPa, whereas the liquid dynamic viscosity and the surface tension were measured at 298.15 K and 101.3 kPa.

According to experimental determinations, it is possible to conclude that the explored vapor–liquid phase equilibria of the ternary mixture positively deviate from Raoult's law, showing zeotropic behavior. For liquid dynamic viscosity and surface tension, no ternary stationary points were detected under the conditions analyzed. The experimental measurements are fully predicted using the PC-SAFT EoS coupled with the FVT and the LGT theories, which allowed predicting the phase equilibria with an overall deviation of 0.66% in temperature and 2.92% in vapor mole fraction of ethanol and 3.55% in vapor mole fraction of DEC, whereas the liquid dynamic viscosity with 12.91%, and surface tension with 2.69%. Considering the theoretical results, it is possible to state that the PC-SAFT EoS, coupled with the FVT and LGT theories, provides a reliable approach for extrapolating phase equilibria, liquid dynamic viscosity, and surface tension to other thermodynamic conditions.

Author contributions

Ariel Hernández: conceptualization (equal), software (lead), investigation (equal), formal analysis (equal). Marcela Cartes: conceptualization (equal), investigation (equal), experimental determinations (lead), methodology (equal), formal analysis (equal), validation (equal), data curation (lead), writing – review & editing (equal). Andrés Mejía: conceptualization (equal), investigation (equal), methodology (equal), formal analysis (equal), validation (equal), writing – review & editing (equal), funding acquisition (lead).

Conflicts of interest

The authors declare no competing financial interest.

Data availability

The data supporting this article have been included as part of the main text.

Acknowledgements

This work was financed by the Chilean National Agency for Research and Development (Agencia Nacional de Investigación y Desarrollo de Chile, ANID) under FONDECYT Project 1230654. A.H acknowledges the economic support given by the UDLA.

Notes and references

1 USEIA, *International Energy Outlook*, 2023, https://www.eia.doe.gov/oiaf/ieo/, accessed: 2026-01-31.

2 Energy Institute, Statistical Review of World Energy, 2025, https://www.energyinst.org/statistical-review, accessed: 2026-01-31.
3 A. Demirbas, *Biodiesel. A Realistic Fuel Alternative for Diesel Engines*, Springer-Verlag, Spain, 2008.
4 J. G. Speight, *Hydrocarbon Biorefinery: Sustainable Processing of Biomass for Hydrocarbon Biofuels*, Royal Society of Chemistry, 1st edn, 2011.
5 *Biorefinery of Alternative Resources: Targeting Green Fuels and Platform Chemicals*, ed. S. Nanda, D.-V. N. Vo and P. K. Sarangi, Springer, Singapore, 2020.
6 *Handbook of Fuels: Energy Sources for Transportation*, ed. B. Elvers and A. Schytze, Wiley-VCH, 2nd edn, 2021.
7 *Hydrocarbon Biorefinery: Sustainable Processing of Biomass for Hydrocarbon Biofuels*, ed. S. K. Maity, K. Gayen and T. K. Bhowmick, Elseviery, 2021.
8 K. Watanabe, N. Yamagiwa and Y. Torisawa, *Org. Process Res. Dev.*, 2007, **11**, 251–258.
9 Y. Roman-Leshkov, C. J. Barrett, Z. Liu and J. Dumesic, *Nature*, 2007, **447**, 982–985.
10 Y. Ren, Z. Huang, H. Miao, Y. Di, D. Jiang, K. Zeng, B. Liu and X. Wang, *Fuel*, 2008, **87**, 2691–2697.
11 M. Kozak, J. Merkisz, P. Bielaczyc and A. Szczotka, The influence of oxygenated diesel fuels on a diesel vehicle PM/NO_x emission trade-off, *Search Technical Papers*, 2009.
12 K. Shukla and V. C. Srivastava, *RSC Adv.*, 2016, **6**, 32624–326245.
13 M. Pan, W. Qian, Z. Zheng, R. Huang, X. Zhou, H. Huang and M. Li, *Fuel*, 2019, **257**, 115920.
14 G. Yang, Q. Wang, L. Li, D. Lyu, H. Lin and D. Han, *Fuel*, 2025, **386**, 134221.
15 G. Dechema, *Gesellschaft für Chemische Technik und Biotechnologie e.V.*, Frankfurt am Main, DETHERM, 2025, https://i-systems.dechema.de/index.php/.
16 A. Hernández, M. Cartes and A. Mejía, *J. Chem. Eng. Data*, 2024, **69**, 639–649.
17 M. Cartes, M. Morales, J. M. Uceda and A. Mejía, *J. Chem. Eng. Data*, 2025, **70**, 4569–4581.
18 J. Gross and G. Sadowski, *Ind. Eng. Chem. Res.*, 2001, **40**, 1244–1260.
19 J. Gross and G. Sadowski, *Ind. Eng. Chem. Res.*, 2002, **41**, 5510–5515.
20 A. Allal, M. Moha-Ouchane and C. Boned, *Phys. Chem. Liq.*, 2001, **39**, 1–30.
21 A. Allal, C. Boned and P. Daugé, *Phys. Chem. Liq.*, 2001, **39**, 607–624.
22 Y.-X. Zuo and E. Stenby, *J. Colloid Interface Sci.*, 1996, **182**, 126–132.
23 Y.-X. Zuo and E. Stenby, *J. Chem. Eng. Jpn.*, 1996, **29**, 159–165.
24 J. M. Uceda, M. Morales, M. Cartes and A. Mejía, *J. Chem. Eng. Data*, 2025, **70**, 2371–2385.
25 J. M. Uceda, M. Morales, M. Cartes and A. Mejía, *Fluid Phase Equilib.*, 2025, **587**, 114199.
26 B. N. Taylor and C. E. Kuyatt, NIST Guidelines for Evaluating and Expressing the Uncertainty of NIST Measurement Results Cover, 1994, https://www.nist.gov/pml/nist-technical-note-1297, accessed: 2026-01-31.
27 BIPM, IEC, ISO and OIML, Introduction to the ISO Guide to the Expression of Uncertainty of Measurement (GUM) Electrical calibration, 1995, DOI: 10.59161/JCGM100-2008E, Accessed: 2026-01-31.
28 J. Wisniak, *Ind. Eng. Chem. Res.*, 1993, **32**, 1531–1533.
29 H. Van Ness and M. Abbott, *Classical Thermodynamics of Non-electrolyte Solutions*, McGraw-Hill, 1982.
30 M. L. Michelsen and J. M. Mollerup, *Thermodynamic Models: Fundamentals and Computational Aspect*, Tie-Line Publications, Holte, 2nd edn, 2007.
31 A. Hernández, M. Cartes and A. Mejía, *Fuel*, 2018, **229**, 105–115.
32 A. Hernández, M. Cartes and A. Mejía, *J. Chem. Eng. Data*, 2023, **69**, 639–649.
33 T. Chung, M. Ajlan, L. Lee and K. Starling, *Ind. Eng. Chem. Res.*, 1988, **27**, 671–679.
34 C. Wohlfarth and W. B, in Landolt-Börnstein: Numerical data and functional relationships in science and technology, *New Series Group IV Physical Chemistry*, ed. M. D. Lechner, Springer Verlag, 1997, vol. 2008, p. 2018.
35 A. Hernández, M. Morales, M. Cartes and A. Mejía, *J. Chem. Eng. Data*, 2025, **70**, 4615–4624.
36 I. Huenuvil-Pacheco, M. Cartes and A. Mejía, *Sustainable Energy Fuels*, 2025, **9**, 4959–4973.
37 V. Diky, R. D. Chirico, M. Frenkel, A. Bazyleva, J. W. Magee, E. Paulechka, A. Kazakov, E. W. Lemmon, C. D. Muzny, A. Y. Smolyanitsky, S. Townsend and K. Kroenlein, *Thermo Data Engine (TDE) Version 10.1 (Pure Compounds, Binary Mixtures, Ternary Mixtures and Chemical Reactions). NIST Standard Reference Database 103b. Thermodynamics Research Center (TRC), Applied Chemicals and Material Division. Standard Reference Data Program*, National Institute of Standards and Technology (NIST), 2016.
38 A. Rodríguez, J. Canosa, A. Domínguez and J. Tojo, *J. Chem. Eng. Data*, 2003, **48**, 86–91.
39 J. Sinor and J. Weber, *J. Chem. Eng. Data*, 1960, **5**, 243–247.
40 A. Rodríguez, J. Canosa, A. Domínguez and J. Tojo, *J. Chem. Eng. Data*, 2002, **47**, 1098–1102.
41 A. Rodríguez, J. Canosa, A. Domínguez and J. Tojo, *J. Chem. Eng. Data*, 2004, **49**, 157–162.
42 M. Cartes, G. Chaparro and G. A. A. Mejía, *J. Mol. Liq.*, 2022, **359**, 119353.
43 A. Rodríguez, J. Canosa, A. Domínguez and J. Tojo, *J. Chem. Eng. Data*, 2003, **48**, 146–151.
44 B. Giner, A. Villares, S. Martin, H. Artigas and C. Lafuente, *J. Chem. Eng. Data*, 2007, **52**, 1904–1907.
45 Z. J. West, T. Yamada, C. R. Bruening, R. L. Cook, S. S. Mueller, L. M. Shafer, M. J. DeWitt and S. Zabarnick, *Energy Fuels*, 2018, **32**, 1166–1178.

